

Accurate Chemistry Collection: Coupled cluster atomization energies for broad chemical space

Sebastian Ehlert^{1,†,*}, Jan Hermann^{1,†,*}, Thijs Vogels¹, Victor Garcia Satorras¹, Stephanie Lanius¹, Marwin Segler¹, Derk P. Kooi¹, Kenji Takeda², Chin-Wei Huang¹, Giulia Luise¹, Rianne van den Berg¹, Paola Gori-Giorgi¹, Amir Karton^{1,3,*}

[†]These authors contributed equally and are ordered randomly.

¹*Microsoft Research, AI for Science*

²*Microsoft Research, Accelerator*

³*University of New England, School of Science and Technology*

*sehlert@microsoft.com, jan.hermann@microsoft.com, amir.karton@une.edu.au

Abstract Accurate thermochemical data with sub-chemical accuracy (i.e., within ± 1 kcal mol⁻¹ from sufficiently accurate experimental or theoretical reference data) is essential for the development and improvement of computational chemistry methods. Challenging thermochemical properties such as heats of formation and total atomization energies (TAEs) are of particular interest because they rigorously test the ability of computational chemistry methods to accurately describe complex chemical transformations involving multiple bond rearrangements. Yet, existing thermochemical datasets that confidently reach this level of accuracy are limited in either size or scope. Datasets with highly accurate reference values include a small number of data points, and larger datasets provide less accurate data or only cover a narrow portion of the chemical space. The existing datasets are therefore insufficient for developing data-driven methods with predictive accuracy over a large chemical space. The Microsoft Research Accurate Chemistry Collection (MSR-ACC) will address this challenge. Here, it offers the MSR-ACC/TAE25 dataset of 76,879 total atomization energies obtained at the CCSD(T)/CBS level via the W1-F12 thermochemical protocol. The dataset is constructed to exhaustively cover chemical space for all elements up to argon by enumerating and sampling chemical graphs, thus avoiding bias towards any particular subspace of the chemical space (such as drug-like, organic, or experimentally observed molecules). With this first dataset in MSR-ACC, we enable data-driven approaches for developing predictive computational chemistry methods with unprecedented accuracy and scope.

Background & summary

The enthalpy of formation is the most fundamental thermodynamic property of a molecule, from which many other thermodynamic properties are derived, for example, reaction and combustion enthalpies, bond dissociation energies, Gibbs-free energies of formation, and equilibrium constants. The enthalpy of formation—i.e., the energy change associated with forming a molecule from its constituent elements in their standard states—is cognate to the total atomization energy (TAE), which is the energy required to break down a molecule into its constituent atoms in the gas phase. These two thermochemical properties are readily interconverted via the atomic enthalpies of formation at 0 K. From a theoretical perspective, the TAEs provide a fundamental reference for determining rigorous error bars for electronic structure theories.^{1–6} The reason for this is not just because the TAE is the most fundamental thermodynamic quantity, but because the TAE is one of the most challenging thermodynamic properties for electronic structure methods. It is well established that thermochemical transformations become increasingly more challenging for approximate electronic structure as they conserve less of the chemical environments between reactants and products.^{7–19} For example, the performance of any approximate electronic structure method is expected to improve along the reaction hierarchy:

atomization \rightarrow isogyric \rightarrow isodesmic \rightarrow hypohomodesmotic \rightarrow homodesmotic \rightarrow hyperhomodesmotic

This improvement is due to progressively more systematic error cancellation between reactants and products occurring along this series.^{7,11,15} Thus, TAEs, which involve the complete dissociation of a molecule into its constituent atoms, represent the most extreme scenario where there is no conservation of the chemical environments between reactants and products. It follows that evaluating the performance of electronic structure methods against TAEs provides upper-bound errors, and the performance for less challenging chemical systems and properties should be improved along this series. Therefore, the primary thermochemical property that we consider in the Microsoft Research Accurate Chemistry Collection (MSR-ACC) is the TAE for a set of highly

diverse set of 76,879 closed-shell systems with up to five non-hydrogen atoms up to argon that are not dominated by nondynamical correlation effects.

Over the past two decades, a number of high-level theoretical datasets for TAEs and heats of formation have been developed. They include the W4 series of datasets, which include 100 (W4-08),²⁰ 140 (W4-11),⁹ and 200 (W4-17)²¹ TAEs of small compounds containing H, B, C, N, O, F, Al, Si, P, S, and Cl. These TAEs are calculated at the full configuration interaction (FCI) complete basis-set (CBS) limit using the W4 composite wavefunction method (or variants thereof).^{22–25} The computational cost of these calculations limits the size and number of systems that can be included in these high-level datasets. Whilst these datasets comprise highly accurate theoretical TAEs, they are limited to prototypical organic and inorganic bonding situations, with a relatively small number of systems containing multiple functionalities in the same molecule. Despite being small, the advantage of such high-level datasets is that they can include multireference systems, since W4 theory has been found to provide confident sub-kJ/mol accuracy even for highly multireference systems such as C₂, O₃ and F₂O₂.^{9,22–26} Moving to computationally more economical coupled-cluster methods, namely with single, double, and quasiperturbative triple excitations (CCSD(T)),²⁷ allows for the calculation of datasets with many more molecules. In a tour de force study, Narayanan et al.²⁸ calculated G4(MP2) energies for 133k organic species (composed of H, C, N, O, and F) with up to 9 non-hydrogen atoms in the GDB-9 dataset (GDB9-G4MP2).²⁹ The G4(MP2) method^{30,31} is a computationally efficient composite wavefunction method, which calculates the CCSD(T) energy in conjunction with the small 6-31G(d) basis set and includes a second-order Möller-Plesset (MP2) perturbation theory basis set correction term calculated in conjunction with a triple- ζ basis set. To account for deficiencies in the theoretical model, G4(MP2) theory includes an empirical 'higher-level correction' (HLC) term. A major advantage of the G4(MP2) method is that it is applicable to large organic systems, such as large polycyclic aromatic hydrocarbons and fullerenes.^{17,32–35} However, for nonstandard bonding situations and for systems that are not well-represented in the experimental G3/05 training set,² G4(MP2) may not achieve chemical accuracy.^{36–41} Composite wavefunction methods such as Wn,⁴² Wn-F12,⁴³ and WnX⁴⁴ ($n = 1, 2$), overcome these limitations by extrapolating the Hartree-Fock, CCSD, and (T) components separately to the CBS limit using relatively large Gaussian basis sets and in addition accelerating the basis set convergence using explicitly correlated techniques. These higher-level CCSD(T)-based composite wavefunction methods also include a core-valence (CV) correction, which is not explicitly included in G4(MP2) theory. Recently, higher-level CCSD(T)-based composite wavefunction methods have been used to generate datasets of heats of formation and TAEs.^{45–47} However, these datasets are mostly limited to organic systems such as those already covered by the GDB9-G4MP2 dataset of Narayanan et al.²⁸ Khan et al.⁴⁸ have also recently published the VQM24 dataset of chemically diverse molecules from the first two rows of the periodic table, and labeled the subset of the 10k smallest molecules with up to 4 non-hydrogen atoms with single-determinant diffusion quantum Monte Carlo (DMC). However, DMC with a single-determinant Slater–Jastrow ansatz, while being a wavefunction method, is insufficiently accurate⁴⁹ for atomization energies, with mean absolute error on the G1 dataset⁵⁰ of ~ 3 kcal/mol, and can only be made more accurate through much more expensive multideterminant ansatzes.

A significant gap in the literature is thus the absence of a chemical dataset covering a broad and diverse set of TAEs for organic and inorganic compounds from the first and second rows of the periodic table at sub-chemical accuracy. As a chemical dataset encompasses more elements, the accessible chemical space expands exponentially, leading to a dramatic increase in the number of unique bonding patterns and the combination of these bonding patterns with various functional groups within the same molecule. In the present work, we construct a chemical dataset, designated MSR-ACC/TAE25, that is composed from all elements of the periodic table up to argon excluding rare-gas atoms (i.e., H, Li, Be, B, C, N, O, F, Na, Mg, Al, Si, P, S, and Cl). Importantly, this dataset is not biased towards a specific chemical subspace (e.g., organic, inorganic, or experimentally observed molecules). The final dataset includes 76,879 charge-neutral closed-shell systems with up to five non-hydrogen atoms that are not dominated by nondynamical correlation effects. To our knowledge, such an extensive dataset of CCSD(T)-based TAEs has not been generated to date. This new dataset opens the way for developing and evaluating generally applicable machine-learning, DFT, and semi-empirical methods.

Methods

Structure generation

The molecular geometries were generated to systematically cover chemical space for elements of the first two rows of the periodic table (H–Ar) excluding the rare-gas atoms. The initial structures were generated with UFF⁵¹ using OpenBabel⁵² to convert SMILES to 3D geometries (Fig. 1a). The resulting structure guess was optimized using GFN2-xTB⁵³ with the *xtb*⁵⁴ program package and reoptimized using r²SCAN-3c⁵⁵ and refined using B3LYP-D3(BJ)^{56,57}/def2-TZVPP (as prescribed by the W1 protocol) with the Orca⁵⁸ program package. In each optimization step, structures were compared with a global index to find duplicates based on the molecular graph⁵⁹ and the total atomization energy at the respective level of theory. Importantly, all the species in the

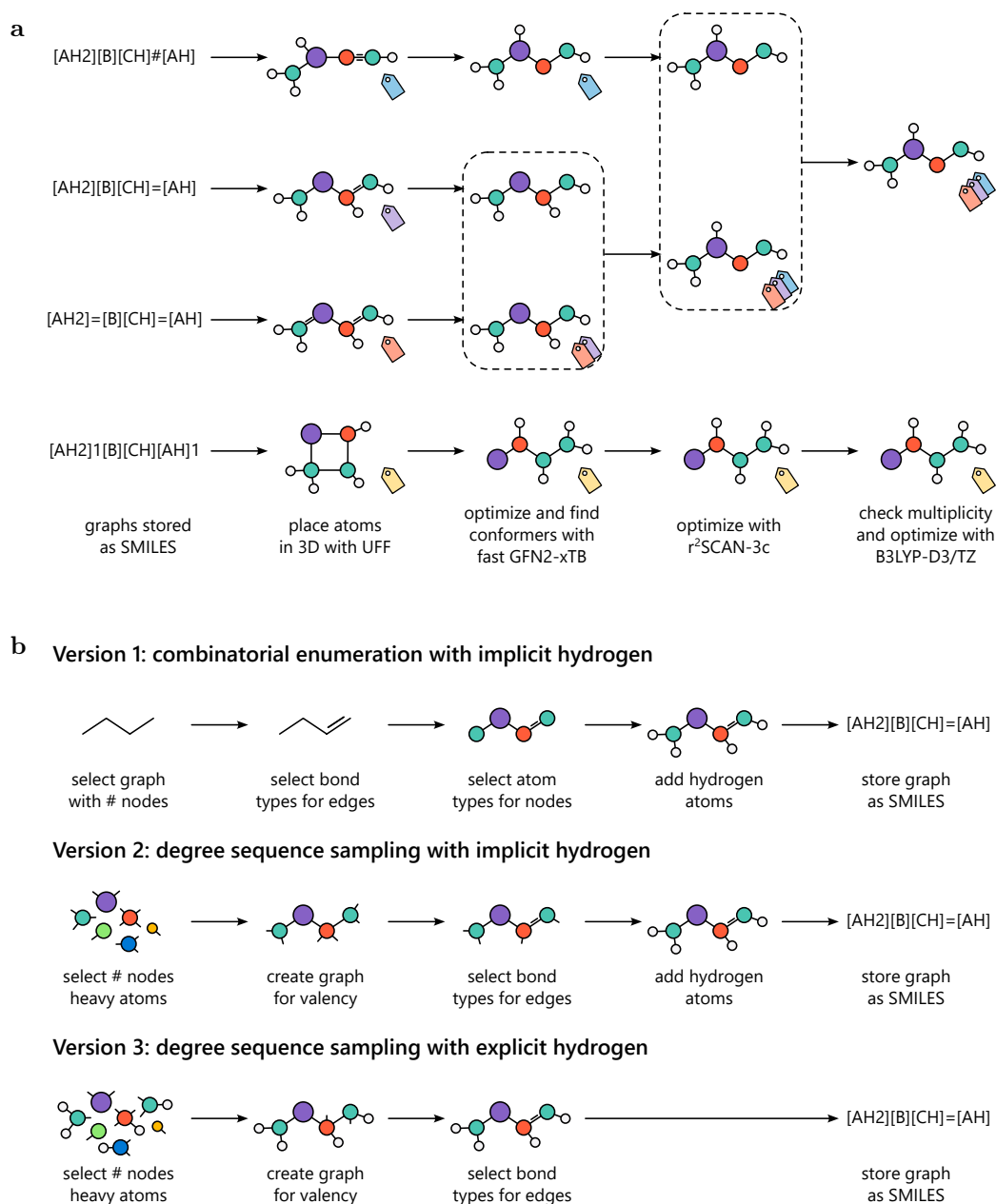


Figure 1: End-to-end molecular structure generation. (a) From molecular graphs to final B3LYP-D3(BJ)/def2-TZVPP optimized structures. Atoms are placed using UFF initially and then optimized using GFN2-xTB which also samples the conformational space. Finally, the geometry is optimized using a meta-GGA (r²SCAN-3c) and a hybrid functional (B3LYP). Spin states are checked at the B3LYP level of theory. (b) Three methods used for generating new molecular graphs. (1) Combinatorial enumeration of all possible graphs, bond types, and atom types before implicitly adding hydrogen atoms. (2) Uses a degree sequence sampling algorithm to create a graph from a sequence of nodes with a maximum valence, bonds are permuted within the maximum valence of the nodes and hydrogen atoms are accounted implicitly. (3) Differs from the previous algorithm by including explicit hydrogen atoms with the nodes already saturating part of the valence.

dataset were verified to be equilibrium structures by confirming they have all-real harmonic frequencies at the same level of theory.

To ensure that the dataset contains only molecules in the electronic ground state, we filter out structures for which the singlet–triplet gap S_0 – T_1 is positive according to B3LYP/def2-TZVPP—this filters out ~5% of all molecules we find. To select the structures which can be safely treated with CCSD(T)-based composite wavefunction protocols, the fraction of TAE accounted for by the parenthetical connected triple excitations (%TAE[(T)]) is computed at the CCSD(T)/6-31G(d) level of theory, all structures with more than 6% %TAE[(T)]

were not considered for labeling. This led to exclusion of additional $\sim 5\%$ of the generated structures. We later verified that the %TAE[(T)] diagnostic taken from W1-F12 theory also does not exceed 6%. Finally, we filter out all structures that have dissociated to more than one covalently bound fragment. We determine the molecular graph through a combination of the bond model of GFN-FF⁵⁹ and a simple heuristic based on a sum of covalent radii.

The initial molecular graphs were generated using different approaches to ensure full coverage of all possible bonding situations (Fig. 1b). First, we use a brute force enumeration of all possible molecular graphs based on bare template graphs for a given number of heavy atoms. While this approach has combinatorial complexity, it allows us to exhaustively enumerate all possible graphs up to four heavy atoms. To reduce the complexity, hydrogen atoms are placed implicitly in this approach. Second, a degree sequence sampling approach is used where candidate graphs are considered from a list of atoms with a degree up to the respective open valence. The resulting bare graphs were dressed with different bond types (single, double, triple), respecting the maximum valence for each atom. The degree sequence sampling was performed once with implicitly added hydrogen atoms and once with explicit hydrogen atoms in the degree sampling step. Third, an autoregressive model based on a GPT2 transformer architecture was used for predicting new molecular graphs. The autoregressive model was trained on all input graphs which could be successfully converted and optimized at B3LYP-D3(BJ)/def2-TZVPP level of theory in SMILES format and sampled for novel graphs which were not part of the training data. This exhaustive generation of molecules can be considered a bottom-up counterpart to the top-down fragment extraction of Huang and von Lilienfeld⁶⁰.

For all structures we evaluate a range of electronic structure methods, including semi-empirical methods GFN1-xTB⁶¹ and GFN2-xTB,⁵⁴ composite electronic structure methods PBEh-3c,⁶² B97-3c,⁶³ r²SCAN-3c,⁵⁵ (meta-)GGAs B97M-V⁶⁴ and r²SCAN-D3(BJ),⁶⁵ (range-separated) hybrid functionals B3LYP-D3(BJ),^{56,57} M06-2X,⁶⁶ ω B97X-V,⁶⁷ and ω B97M-V,⁶⁸ and double hybrid functionals revDSD-PBEP86-D3(BJ)⁶⁹ and ω B97X-2.⁷⁰

Labeling with the composite W1-F12 protocol

Using the fully optimized B3LYP-D3(BJ)/def2-TZVPP structures, we obtain the nonrelativistic, all-electron CCSD(T)/CBS TAE using the high-level W1-F12 composite wavefunction protocol.⁴³ W1-F12 theory is an explicitly correlated⁷¹⁻⁷³ version of the original W1 theory.⁴² The computational details of W1-F12 theory have been specified and rationalized in great detail elsewhere.⁴³ In brief, the Hartree-Fock (HF) energy is extrapolated to the complete basis-set limit from the cc-pVDZ-F12 and cc-pVTZ-F12 basis sets,⁷⁴ using the $E(L) = E_\infty + A/L^\alpha$ two-point extrapolation formula, with $\alpha = 5$. The complementary auxiliary basis set (CABS) singles correction is included in the Hartree-Fock (HF) energy.⁷⁵⁻⁷⁷ The valence CCSD-F12 correlation energy (denoted by Δ CCSD hereinafter) is extrapolated from the same basis sets, using an optimal extrapolation exponent for elements up to argon of $\alpha = 3.67$. The valence parentetical connected triple excitations (denoted by Δ (T)) is obtained from standard CCSD(T) calculations, as is the case in W1w theory.^{22,42} Specifically, the Δ (T) component is extrapolated from the jul-cc-pV(D+d)Z and jul-cc-pV(T+d)Z basis sets using the above two-point extrapolation formula with $\alpha = 3.22$.⁷⁸⁻⁸¹ The CCSD inner-shell contribution is calculated with the core-valence weighted correlation-consistent cc-pwCVTZ basis set of Peterson and Dunning,⁸² while the (T) inner-shell contribution is calculated with the cc-pwCVTZ basis set without the f functions. Since we are primarily interested in assessing the performance of nonrelativistic computational chemistry methods on the electronic potential energy surface, the scalar relativistic, spin-orbit, and diagonal Born-Oppenheimer corrections are not considered in the present work.

We have labeled all found molecules with up to 4 non-hydrogen atoms, and a smaller sample of all found molecules with 5 non-hydrogen atoms.

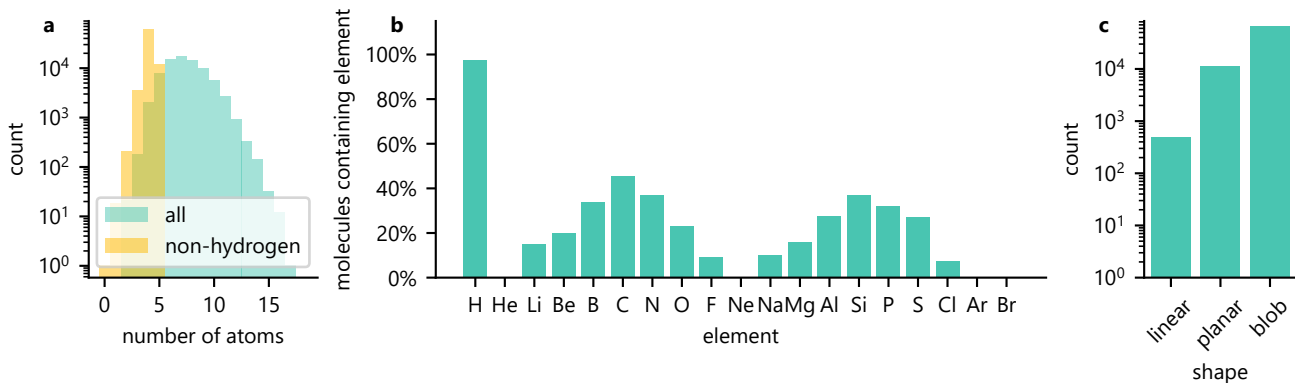
Data record

The data records for 76,879 molecules of the first public version of MSR-ACC are available in Zenodo (<https://doi.org/10.5281/zenodo.15387280>) under the CDLA-Permissive-2.0 license. To aid machine-learning applications, we release also training and validation subsets of the full dataset, which constitute canonical 99% and 1% splits, respectively, of MSR-ACC/TAE25 after removing the overlap with popular W4-17 and GMTKN55 benchmark sets. The overlap contains any atomization reaction where the reconstructed molecular graph of the molecules match.

Molecules are formatted using the QCSchema standard, including the Cartesian coordinates in bohr (`geometry` field), element symbols (`symbols` field), total charge (`molecular_charge` field) and spin state (`molecular_multiplicity` field). The `extras` field of each molecule contains the W1-F12 atomization energy labels

Table 1: Labels included in the `extras` field of the data records.

Key	Description	Unit
<code>graph:all</code>	Connectivity of all atoms	list of indices (0-based)
<code>graph:non-h</code>	Connectivity of all non-hydrogen atoms	list of indices (0-based)
<code>tae@{method}</code>	Total atomization energy	hartree
<code>tae:frac[(T)]@{method}</code>	%TAE[(T)] as a fraction	1
<code>singlet-triplet-gap-s0-t1@{method}</code>	Singlet-triplet gap S_0-T_1	hartree
<code>tae[{component}]@w1-f12</code>	Component of the W1-F12 TAE	hartree

**Figure 2:** Elemental and structural distributions. (a) Molecular size as atom count. (b) Elemental occurrence. Hydrogen is present in 97.6% of molecules. (c) General 3D shape of the molecules.

(`tae@w1-f12`) as well as additional information including molecular graphs, DFT atomization energies, singlet-triplet gaps, and W1-F12 energy components described in Table 1.

Technical validation

Figure 2 gives an overview of basic structural distributions over MSR-ACC/TAE25. The molecular sizes range from zero (H_2) to five non-hydrogen atoms and from 2 to 17 (isopentane) atoms including hydrogen. Defining organic systems as molecules containing at least one carbon atom, there are 45.5% organic systems and 54.5% inorganic systems. Thus, similarly to the much smaller and chemically less diverse W4-17 dataset, there is a similar representation of organic and inorganic systems. The most represented elements in the dataset are:

$$C > N \text{ and } Si > B \text{ and } P > S \text{ and } Al > O > Be > Mg > Li > Na > F > Cl$$

Importantly, about 75% of the systems are mixed second/third-period species, 17% are pure second-period systems, and about 8% are pure third-period systems. The geometry of the molecules spans linear (0.6%), planar (14.9%) and general 3D structures (84.5%).

The elemental composition of the molecules in MSR-ACC gives rise to a diverse bond types, with many molecules involving nontraditional bonding situations. Overall, there are 301k bonds between non-hydrogen atoms in MSR-ACC/TAE25 according to our bond heuristic, covering all possible combinations of elements in the first two rows except for F-F. The occurrence of element pairs involved in bonding follows the pattern that could be expected from typical valencies of individual elements (Figure 3a). Notable outliers in occurrence are pairs of typically monovalent elements: H-H (only once in H_2), H-halogen (21), Cl-halogen (10), and F-F (none, as F_2 is associated with %TAE[(T)] > 6%). This can be contrasted to two other large atomization energy datasets labeled with ab-initio wavefunction methods. VQM24/DMC follows the same bond distributions with non-hydrogen elements from groups 1, 2, and 13 (Li, Na, Be, Mg, B, Al) omitted and Br added (following the same pattern as other halogens). GDB-9 is severely restricted in diversity by its focus on organic drug-like molecules, resulting in only C-C, C-N, C-O, C-F, N-N, and N-O non-hydrogen bonds, with the latter three occurring with low relative frequency.

A different metric of chemical diversity is obtained by counting unique 1st-neighbor environments in the molecular graphs for each element (Figure 3b). In the full dataset, all elements except for H and halogens occur in ~ 1000 unique chemical environments, while H and halogens occur in ~ 100 unique chemical environments. Hydrogen gains this diversity through various two-electron three-centric bonds with one atom from groups 1, 2, and 13, and some other non-hydrogen element. When restricting to molecules with no non-hydrogen atom from groups 1,

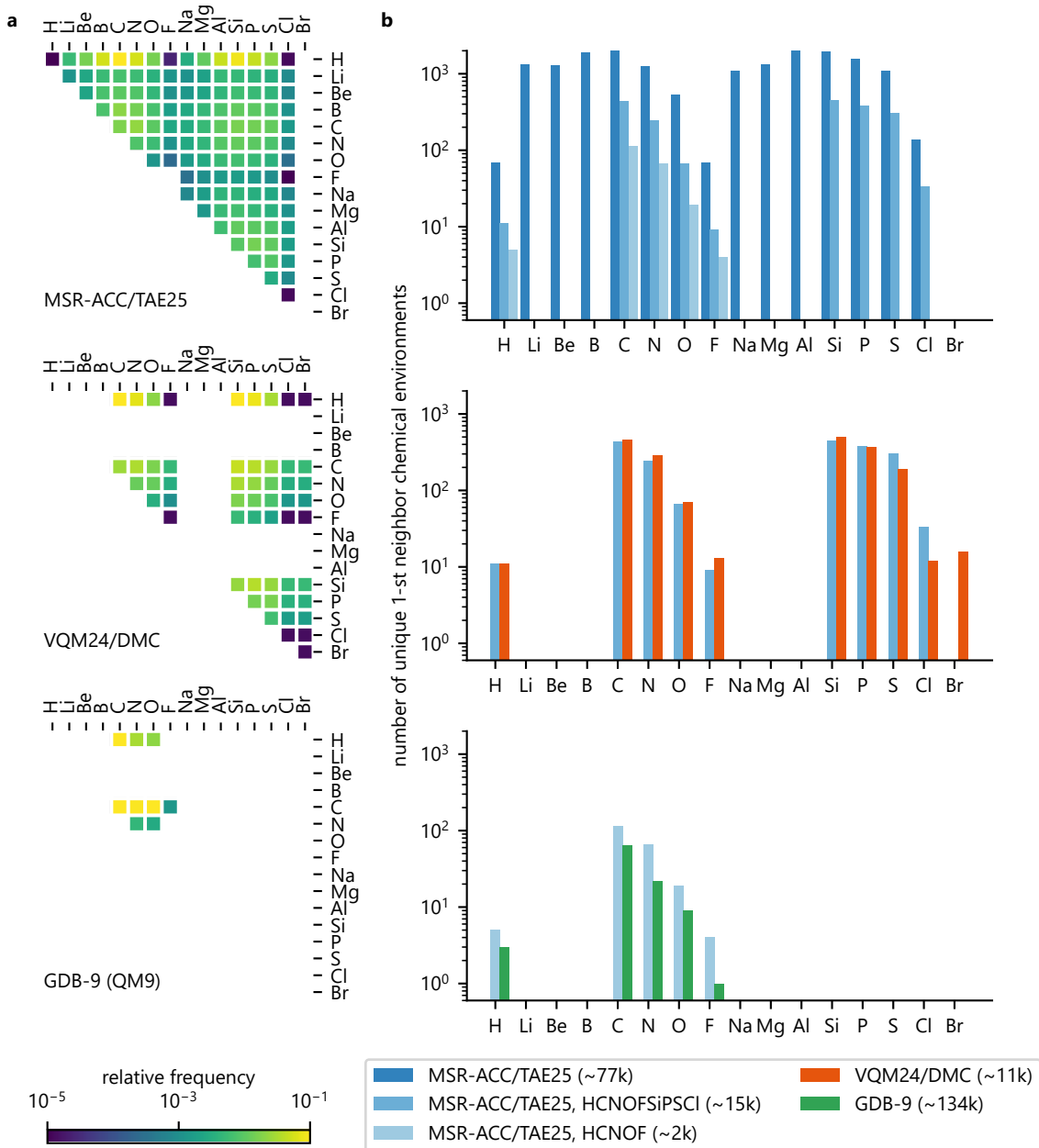


Figure 3: Reconstructed molecular graphs compared across three datasets: MSR-ACC/TAE25, VQM24/DMC, and GDB-9 (also known as QM9). Graphs are reconstructed from 3D structures using a bond model from GFN-FF and a simple heuristic based on a sum of covalent radii. **(a)** Distribution of element pairs in bonds. **(b)** Unique 1-st neighbor environments per element. Subsets of MSR-ACC/TAE25 constrained to elemental subspaces are also shown.

2, and 13, the number of unique chemical environments drops by half an order of magnitude, and its distribution over elements is remarkably similar to VQM24/DMC. This indirectly verifies that the structure generation for both datasets exhaustively covers all possible local chemical environments in the respective elemental spaces. When further restricting to the HCN OF subset, we find that the number of unique environments in MSR-ACC is still 2-3 times larger than in GDB-9, owing to covering more than just 'drug-like' organic chemistry.

Yet another validation of the coverage of the chemical space is comparison of the overlap between MSR-ACC/TAE25 and the closed-shell single-referential subset of W4-17 up to 4 non-hydrogen atoms, which we expect to be covered exhaustively. Indeed we find that only two molecules from this W4-17 subset are missing in MSR-ACC/TAE25: diborane, B_2H_6 , which due to its uniqueness cannot be constructed by our molecular graph generation, and cyclobutadiene, C_4H_4 , likely due to its instability, since we did find two dozen of its other isomers.

It is well established that the CCSD(T) method cannot generally achieve chemical accuracy for systems dominated

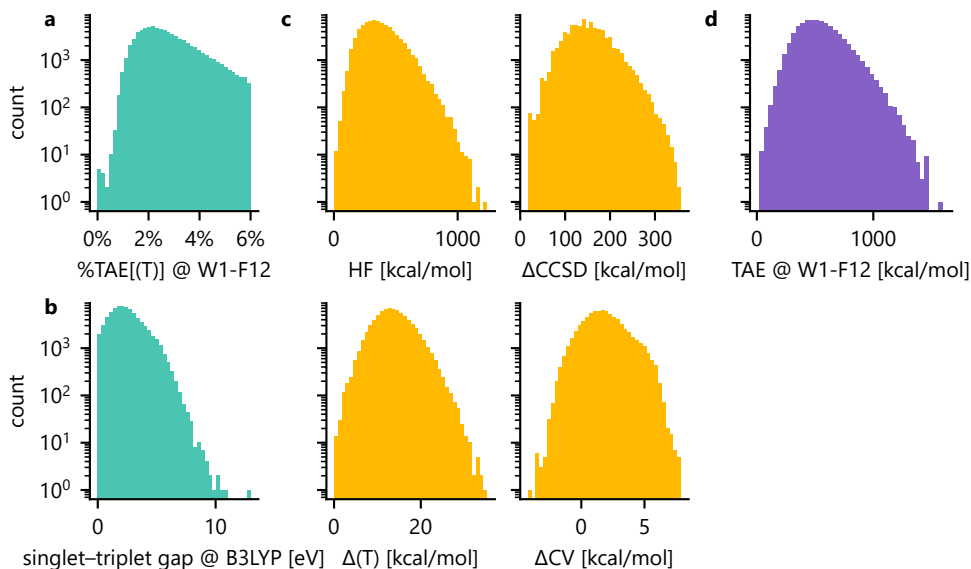


Figure 4: Energetic distributions. (a) Multireference diagnostic %TAE[(T)]. (b) Vertical singlet-triplet gaps S_0-T_1 from B3LYP. (c) All four components of the W1-F12 total atomization energy. (d) Reference W1-F12 total atomization energy.

by moderate-to-severe nondynamical correlation effects.^{9,21–26,83–87} It is therefore essential to estimate the contributions to the TAEs from post-CCSD(T) excitations. A highly successful a priori predictor for such contributions is the so-called %TAE[(T)] diagnostic,^{9,22,23} which is defined as the percentage of the TAE accounted for by parenthetical connected triple excitations:

$$\%TAE[(T)] = \frac{TAE[CCSD(T)] - TAE[CCSD]}{TAE[CCSD(T)]}$$

where TAE[CCSD] and TAE[CCSD(T)] are the TAEs calculated at the CCSD and CCSD(T) levels. This simple multireference diagnostic is particularly well suited for eliminating systems with significant post-CCSD(T) contributions to the TAEs. It has been suggested that %TAE[(T)] values up to $\sim 5\%$ indicate that post-CCSD(T) contributions to the TAEs should not exceed $\sim 0.5 \text{ kcal mol}^{-1}$.²³ In the present work, we have chosen to exclude all systems with %TAE[(T)] $> 6\%$. The distribution of %TAE[(T)] (Fig. 4a) therefore ends sharply at 6%, while peaking at $\sim 2\%$ and tapering off towards 0%. The second major filtering criterion is positive vertical singlet-triplet S_0-T_1 gap, in order to have only molecules in their electronic ground states. The distribution of the S-T gap (Fig. 4b) therefore ends sharply at 0 eV, peaks at $\sim 2 \text{ eV}$, and tapers off to $\sim 10 \text{ eV}$.

Fig. 4c gives an overview of the HF, ΔCCSD , $\Delta(T)$, and ΔCV contributions to the W1-F12 TAEs. The HF component spreads over a wide range from 1.1 to $1238.8 \text{ kcal mol}^{-1}$. We note, however, that small HF TAEs below $32.5 \text{ kcal mol}^{-1}$ are obtained for only 12 systems, nearly all of which consist of Li bonding with Na, Be, or Mg. The overall all-electron CCSD(T)/CBS TAEs for these 12 systems are also relatively small and range between 20.1 and $59.9 \text{ kcal mol}^{-1}$. HF TAEs above $1000 \text{ kcal mol}^{-1}$ are obtained for 42 systems, nearly all of which contain 4–5 carbon atoms. We note that there is no apparent correlation between the HF component and the number of non-hydrogen atoms, however, the squared correlation coefficient between the total number of atoms and the HF component is $R^2 = 0.759$.

The ΔCCSD component spreads over a wide range of $340 \text{ kcal mol}^{-1}$ from 18.4 to $358 \text{ kcal mol}^{-1}$. The largest 40 ΔCCSD contributions range between 327 and $358.1 \text{ kcal mol}^{-1}$. Most of these systems are nitrogen-rich species. The systems with the smallest ΔCCSD contributions are dominated by beryllium compounds. We note that overall, for the 76,879 systems in the dataset, there is a noticeable but weak statistical correlation between ΔCCSD component and the number of valence electrons, with $R^2 = 0.616$.

The $\Delta(T)$ component varies between 0.0 and $35.3 \text{ kcal mol}^{-1}$. The lowest $\Delta(T)$ contributions are obtained, as expected, for lithium and sodium systems. Excluding the systems with only two valence electrons (H_2 , HLi, HNa, LiNa) for which the $\Delta(T)$ contribution is zero by definition, the lowest 40 $\Delta(T)$ contributions range between 0.0 and $1.7 \text{ kcal mol}^{-1}$. Of these 40 systems, 22 contain either Na or Li, or both, where in most cases there are multiple Li and Na atoms in the same molecule. Similarly to the ΔCCSD component, the largest $\Delta(T)$ contributions are obtained for nitrogen-rich species.

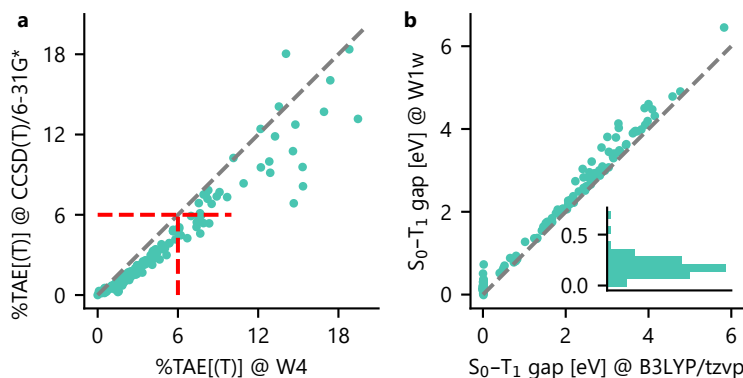


Figure 5: Validation of filtering criteria. **(a)** Multireference descriptor $\%TAE[(T)]$ evaluated on the W4-17 dataset in the small 6-31G(d) basis almost always underestimates the true CBS value (from W4), leading to false negatives but no false positives of multireference character. **(b)** Singlet-triplet gaps are only overestimated by B3LYP, never underestimated. A random sample of molecules with the B3LYP gap close to zero (inset) has the CCSD(T) gap (from W1w) ranging from 0.0 to 0.4 eV.

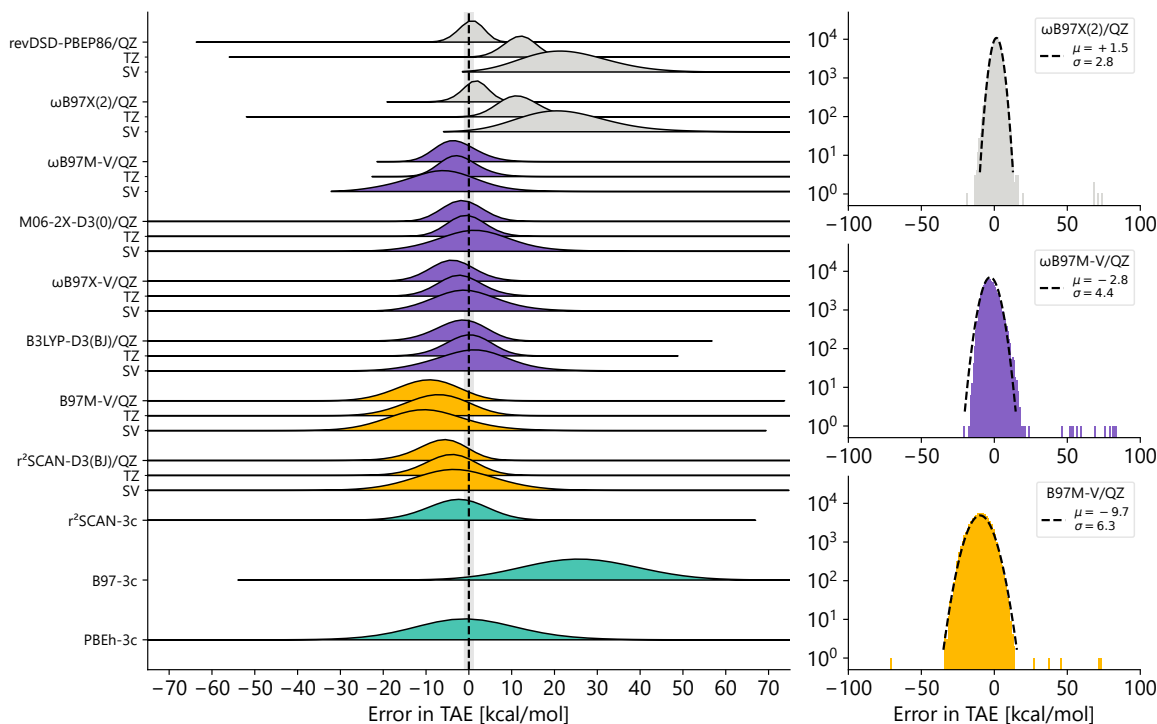


Figure 6: Error distribution of common exchange-correlation (XC) functionals with respect to W1-F12 reference values. The error distribution of each functional is shown in def2-QZVP, def2-TZVP, and def2-SVP from top to bottom, except for composite DFT methods. The error range of ± 1 kcal mol⁻¹ is highlighted as light gray area. Jacob’s ladder rungs are denoted with color. For selected functionals the distribution is replotted in log scale with a fitted normal distribution.

The ΔCV contribution can be either negative or positive, meaning that ΔCV correlation is more or less stabilizing, respectively, in the constituent atoms than in the molecule. Overall, the ΔCV contributions range from -4.2 to $+7.9$ kcal mol⁻¹, where 12% of the ΔCV values are negative and 88% are positive. In line with observations^{23–25} on the W4-17 dataset,²¹ 87.5% of the systems with a negative CV correction contain Al, Si, or both atoms. The resulting TAEs range from 20.1 (LiNa) to 1560 kcal mol⁻¹ (isopentane).

We introduced two primary approximate filtering criteria when constructing MSR-ACC. First, $\%TAE[(T)]$ computed in the small 6-31G(d) basis is used to identify multireference molecules to be filtered out before

labeling them with the much more expensive W1-F12 calculation. We have verified on the W4-17 dataset that this almost never leads to excluding molecules that are in fact single-referential, as the small-basis version of the metric strictly underestimates it (Fig. 5a). It leads to an additional small fraction of molecules being excluded only after the W1-F12 calculations is finished. Second, singlet–triplet gap S_0 – T_1 is approximated by B3LYP/def2-TZVP to exclude molecules with a triplet ground state. We have verified on a random sample of molecules from the dataset against gaps calculated with W1w that B3LYP strictly underestimates the gap (Fig. 5b). This leads to a small fraction of molecules being unnecessarily filtered out that have in fact a singlet ground state, but we consider this worth the saved cost of having to run extra W1-F12 triplet calculations.

Next to the reference W1-F12 values, the dataset contains TAEs from KS-DFT with a number of popular exchange–correlation (XC) functionals. We found that the distribution of errors of all functionals with respect to the reference values follows the normal distribution very closely, which enables us to identify outliers confidently (Fig. 6). This can then serve as an indirect validation of the reference values, where we ensure that that are no case of different XC functionals agreeing among each other on the TAE but disagreeing with W1-F12. The accuracy of the different XC functionals follows the general trends one would expect from the Jacob’s ladder categorization.

Acknowledgments

We acknowledge Microsoft Accelerating Foundation Models Research Program for access to Microsoft Azure cloud compute.

References

- [1] M. K. Sprague and K. K. Irikura. Quantitative estimation of uncertainties from wavefunction diagnostics. *Theor. Chem. Acc.*, 133:1544, 2014.
- [2] L. A. Curtiss, P. C. Redfern, and K. Raghavachari. Assessment of gaussian-3 and density-functional theories on the g3/05 test set of experimental energies. *J. Chem. Phys.*, 123:124107, 2005. doi: 10.1063/1.2039080.
- [3] B. Ruscic, R. E. Pinzon, M. L. Morton, G. von Laszewski, S. J. Bittner, S. G. Nijssure, K. A. Amin, M. Minkoff, and A. F. Wagner. Introduction to active thermochemical tables: Several “key” enthalpies of formation revisited. *J. Phys. Chem. A*, 108:9979–9997, 2004. doi: 10.1021/jp047912y.
- [4] B. Ruscic, R. E. Pinzon, G. von Laszewski, D. Kodeboyina, A. Burcat, D. Leahy, D. Montoya, and A. F. Wagner. Active thermochemical tables: Thermochemistry for the 21st century. *J. Phys.: Conf. Ser.*, 16: 561, 2005. doi: 10.1088/1742-6596/16/1/078.
- [5] L. A. Curtiss, K. Raghavachari, P. C. Redfern, and J. A. Pople. Assessment of gaussian-3 and density functional theories for a larger experimental test set. *J. Chem. Phys.*, 112:7374, 2000.
- [6] L. A. Curtiss, K. Raghavachari, G. W. Trucks, and J. A. Pople. Gaussian-2 theory for molecular energies of first-row and second-row compounds. *J. Chem. Phys.*, 94:7221–7230, 1991. doi: 10.1063/1.460205.
- [7] S. E. Wheeler, K. N. Houk, P. v. R. Schleyer, and W. D. Allen. Hierarchy of homodesmotic reactions for thermochemistry. *J. Am. Chem. Soc.*, 131:2547, 2009. doi: 10.1021/ja808278b.
- [8] A. Karton, D. Gruzman, and J. M. L. Martin. Benchmark Thermochemistry of the $C_n H_{2n+2}$ Alkane Isomers ($n = 2$ –8) and Performance of DFT and Composite Ab Initio Methods for Dispersion-Driven Isomeric Equilibria. *The Journal of Physical Chemistry A*, 113(29):8434–8447, July 2009. ISSN 1089-5639, 1520-5215. doi: 10.1021/jp904369h. URL <https://pubs.acs.org/doi/10.1021/jp904369h>.
- [9] A. Karton, S. Daon, and J. M. Martin. W4-11: A high-confidence benchmark dataset for computational thermochemistry derived from first-principles W4 data. *Chemical Physics Letters*, 510(4-6):165–178, July 2011. ISSN 00092614. doi: 10.1016/j.cplett.2011.05.007. URL <https://linkinghub.elsevier.com/retrieve/pii/S0009261411005616>.
- [10] R. O. Ramabhadran and K. Raghavachari. Theoretical thermochemistry for organic molecules: Development of the generalized connectivity-based hierarchy. *J. Chem. Theory Comput.*, 7:2094, 2011.
- [11] S. E. Wheeler. Homodesmotic reactions for thermochemistry. *WIREs Comput. Mol. Sci.*, 2:204, 2012. doi: 10.1002/wcms.88.
- [12] R. O. Ramabhadran and K. Raghavachari. Connectivity-based hierarchy for theoretical thermochemistry: Assessment using wave function-based methods. *J. Phys. Chem. A*, 116:7531, 2012.

- [13] R. O. Ramabhadran and K. Raghavachari. The successful merger of theoretical thermochemistry with fragment-based methods in quantum chemistry. *Acc. Chem. Res.*, 47:3596, 2014.
- [14] L.-J. Yu and A. Karton. Assessment of theoretical procedures for a diverse set of isomerization reactions involving double-bond migration in conjugated dienes. *Chem. Phys.*, 441:166, 2014.
- [15] A. Karton, P. R. Schreiner, and J. M. L. Martin. Heats of formation of platonic hydrocarbon cages by means of high-level thermochemical procedures. *J. Comput. Chem.*, 37:49, 2016. doi: 10.1002/jcc.23986.
- [16] B. Chan, E. Collins, and K. Raghavachari. Applications ofisodesmic-type reactions for computational thermochemistry. *WIREs Comput. Mol. Sci.*, 11:e1501, 2021. doi: 10.1002/wcms.1501.
- [17] A. Karton and B. Chan. Pah335 – a diverse database of highly accurate ccSD(T) isomerization energies of 335 polycyclic aromatic hydrocarbons. *Chem. Phys. Lett.*, 824:140544, 2023.
- [18] W. J. Hehre, R. Ditchfield, L. Radom, and J. A. Pople. Molecular orbital theory of the electronic structure of organic compounds. v. molecular theory of bond separation. *J. Am. Chem. Soc.*, 92:4796–4801, 1970.
- [19] L. Radom, W. J. Hehre, and J. A. Pople. Molecular orbital theory of the electronic structure of organic compounds. vii. systematic study of energies, conformations, and bond interactions. *J. Am. Chem. Soc.*, 93: 289–300, 1971.
- [20] A. Karton, A. Tarnopolsky, J.-F. Lamere, G. C. Schatz, and J. M. L. Martin. Highly accurate first-principles benchmark data sets for the parameterization and validation of density functional and other approximate methods. derivation of a robust, generally applicable, double-hybrid functional for thermochemistry and thermochemical kinetics. *J. Phys. Chem. A*, 112:12868–12886, 2008.
- [21] A. Karton, N. Sylvetsky, and J. M. L. Martin. W4-17: A diverse and high-confidence dataset of atomization energies for benchmarking high-level electronic structure methods. *Journal of Computational Chemistry*, 38(24):2063–2075, Sept. 2017. ISSN 0192-8651, 1096-987X. doi: 10.1002/jcc.24854. URL <https://onlinelibrary.wiley.com/doi/10.1002/jcc.24854>.
- [22] A. Karton, E. Rabinovich, J. M. L. Martin, and B. Ruscic. W4 theory for computational thermochemistry: In pursuit of confident sub-kJ/mol predictions. *The Journal of Chemical Physics*, 125(14):144108, Oct. 2006. ISSN 0021-9606, 1089-7690. doi: 10.1063/1.2348881. URL <https://pubs.aip.org/jcp/article/125/14/144108/295614/W4-theory-for-computational-thermochemistry-In>.
- [23] A. Karton. A computational chemist’s guide to accurate thermochemistry for organic molecules. *WIREs Comput. Mol. Sci.*, 6:292–310, 2016.
- [24] A. Karton. Quantum mechanical thermochemical predictions 100 years after the Schrödinger equation. In *Annual Reports in Computational Chemistry*, volume 18, pages 123–166. Elsevier, 2022. ISBN 978-0-323-99092-9. doi: 10.1016/bs.arcc.2022.09.003. URL <https://linkinghub.elsevier.com/retrieve/pii/S1574140022000032>.
- [25] A. Karton. Benchmark accuracy in thermochemistry, kinetics, and noncovalent interactions. In R. J. Boyd and M. Yanez, editors, *Comprehensive Computational Chemistry*, volume 1, pages 47–68. Elsevier, 1 edition, 2023. ISBN 9780128232569.
- [26] A. Karton, P. R. Taylor, and J. M. L. Martin. Basis set convergence of post-CCSD contributions to molecular atomization energies. *J. Chem. Phys.*, 127:064104, 2007. doi: 10.1063/1.2755751.
- [27] K. Raghavachari, G. W. Trucks, J. A. Pople, and M. Head-Gordon. A fifth-order perturbation comparison of electron correlation theories. *Chem. Phys. Lett.*, 157:479–483, 1989.
- [28] B. Narayanan, P. C. Redfern, R. S. Assary, and L. A. Curtiss. Accurate quantum chemical energies for 133000 organic molecules. *Chem. Sci.*, 10:7449, 2019.
- [29] R. Ramakrishnan, P. O. Dral, M. Rupp, and O. A. von Lilienfeld. Quantum chemistry structures and properties of 134 kilo molecules. *Scientific Data*, 1(1):140022, Aug. 2014. ISSN 2052-4463. doi: 10.1038/sdata.2014.22. URL <https://www.nature.com/articles/sdata201422>. Publisher: Nature Publishing Group.
- [30] L. A. Curtiss, P. C. Redfern, and K. Raghavachari. Gaussian-4 theory using reduced order perturbation theory. *J. Chem. Phys.*, 127:124105, 2007.

- [31] L. A. Curtiss, P. C. Redfern, and K. Raghavachari. Gn theory. *Wiley Interdiscip. Rev.: Comput. Mol. Sci.*, 1:810, 2011.
- [32] W. Wan and A. Karton. Heat of formation for c60 by means of the g4(mp2) thermochemical protocol through reactions in which c60 is broken down into corannulene and sumanene. *Chem. Phys. Lett.*, 643: 34–38, 2016.
- [33] A. Karton, S. L. Waite, and A. J. Page. Performance of dft for c60 isomerization energies: A noticeable exception to jacob’s ladder. *J. Phys. Chem. A*, 123:257–262, 2019.
- [34] A. Karton. Fullerenes pose a strain on hybrid density functional theory. *J. Phys. Chem. A*, 126:4709–4717, 2022.
- [35] A. Karton and B. Chan. Performance of local g4(mp2) composite ab initio procedures for fullerene isomerization energies. *Comput. Theor. Chem.*, 1217:113874, 2022.
- [36] A. Karton, M. Haasler, and M. Kaupp. Post-CCSD(T) thermochemistry of chlorine fluorides as a challenging test case for evaluating density functional theory and composite ab initio methods. *ChemPhysChem*, 26:e202400750, 2025.
- [37] A. Karton. High-level thermochemistry for the octasulfur ring: A converged coupled cluster perspective for a challenging second-row system. *Chem. Phys. Impact*, 3:100047, 2021.
- [38] L.-J. Yu, S. G. Dale, B. Chan, and A. Karton. Benchmark study of DFT and composite methods for bond dissociation energies in argon compounds. *Chem. Phys.*, 531:110676, 2020.
- [39] A. Kroeger and A. Karton. Thermochemistry of phosphorus sulfide cages: An extreme challenge for high-level ab initio methods. *Struct. Chem.*, 30:1665, 2019.
- [40] F. Sarrami, L.-J. Yu, and A. Karton. Thermochemistry of icosahedral closo-dicboranes: A composite ab initio quantum-chemical perspective. *Can. J. Chem.*, 94:1082–1089, 2016.
- [41] A. Karton, A. Tarnopolsky, and J. Martin. Atomization energies of the carbon clusters C_n ($n = 2-10$) revisited by means of W4 theory as well as density functional, G_n , and CBS methods. *Mol. Phys.*, 107: 977–990, 2009.
- [42] J. M. L. Martin and G. de Oliveira. Towards standard methods for benchmark quality ab initio thermochemistry—w1 and w2 theory. *J. Chem. Phys.*, 111:1843–1856, 1999.
- [43] A. Karton and J. M. L. Martin. Explicitly correlated wn theory: W1-f12 and w2-f12. *J. Chem. Phys.*, 136: 124114, 2012.
- [44] B. Chan and L. Radom. W1x-1 and w1x-2: W1-quality accuracy with an order of magnitude reduction in computational cost. *J. Chem. Theory Comput.*, 8:4259–4269, 2012.
- [45] B. Chan. High-level quantum chemistry reference heats of formation for a large set of c, h, n, and o species in the nist chemistry webbook and the identification and validation of reliable protocols for their rapid computation. *J. Phys. Chem. A*, 126:4981–4990, 2022.
- [46] B. Chan. Reliable quantum-chemistry heats of formation for an extensive set of c-, h-, n-, o-, f-, s-, cl-, br-containing molecules in the nist chemistry webbook. *J. Phys. Chem. A*, 129:3578–3586, 2025.
- [47] A. Karton. A highly diverse and accurate database of 3366 total atomization energies calculated at the CCSD(T)/CBS level by means of W1-F12 theory. *Chem. Phys. Lett.*, 868:142030, 2025.
- [48] D. Khan, A. Benali, S. Y. H. Kim, G. F. von Rudorff, and O. A. von Lilienfeld. Quantum mechanical dataset of 836k neutral closed shell molecules with upto 5 heavy atoms from cnohipsclbr, 2024. URL <https://arxiv.org/abs/2405.05961>.
- [49] M. A. Morales, J. McMinis, B. K. Clark, J. Kim, and G. E. Scuseria. Multideterminant wave functions in quantum monte carlo. *Journal of Chemical Theory and Computation*, 8(7):2181–2188, 2012. doi: 10/f34p94. URL <https://pubs.acs.org/doi/10.1021/ct3003404>.
- [50] L. A. Curtiss, C. Jones, G. W. Trucks, K. Raghavachari, and J. A. Pople. Gaussian-1 theory of molecular energies for second-row compounds. *The Journal of Chemical Physics*, 93(4):2537–2545, 1990. doi: 10.1063/1.458892. URL <https://doi.org/10.1063/1.458892>.

- [51] A. K. Rappe, C. J. Casewit, K. S. Colwell, W. A. I. Goddard, and W. M. Skiff. UFF, a full periodic table force field for molecular mechanics and molecular dynamics simulations. *Journal of the American Chemical Society*, 114(25):10024–10035, Dec. 1992. ISSN 0002-7863. doi: 10.1021/ja00051a040. URL <https://doi.org/10.1021/ja00051a040>. Publisher: American Chemical Society.
- [52] N. M. O’Boyle, M. Banck, C. A. James, C. Morley, T. Vandermeersch, and G. R. Hutchison. Open Babel: An open chemical toolbox. *Journal of Cheminformatics*, 3(1):33, Oct. 2011. ISSN 1758-2946. doi: 10.1186/1758-2946-3-33. URL <https://doi.org/10.1186/1758-2946-3-33>.
- [53] C. Bannwarth, S. Ehlert, and S. Grimme. GFN2-xTB—An Accurate and Broadly Parametrized Self-Consistent Tight-Binding Quantum Chemical Method with Multipole Electrostatics and Density-Dependent Dispersion Contributions. *Journal of Chemical Theory and Computation*, 15(3):1652–1671, Mar. 2019. ISSN 1549-9618. doi: 10.1021/acs.jctc.8b01176. URL <https://doi.org/10.1021/acs.jctc.8b01176>. Publisher: American Chemical Society.
- [54] C. Bannwarth, E. Caldeweyher, S. Ehlert, A. Hansen, P. Pracht, J. Seibert, S. Spicher, and S. Grimme. Extended tight-binding quantum chemistry methods. *WIREs Computational Molecular Science*, 11(2): e1493, 2021. ISSN 1759-0884. doi: 10.1002/wcms.1493. URL <https://onlinelibrary.wiley.com/doi/abs/10.1002/wcms.1493>. _eprint: <https://onlinelibrary.wiley.com/doi/pdf/10.1002/wcms.1493>.
- [55] S. Grimme, A. Hansen, S. Ehlert, and J.-M. Mewes. r2SCAN-3c: A “Swiss army knife” composite electronic-structure method. *The Journal of Chemical Physics*, 154(6):064103, Feb. 2021. ISSN 0021-9606. doi: 10.1063/5.0040021. URL <https://doi.org/10.1063/5.0040021>.
- [56] A. D. Becke. Density-functional thermochemistry. III. The role of exact exchange. *The Journal of Chemical Physics*, 98(7):5648–5652, Apr. 1993. ISSN 0021-9606. doi: 10.1063/1.464913. URL <https://doi.org/10.1063/1.464913>.
- [57] P. J. Stephens, F. J. Devlin, C. F. Chabalowski, and M. J. Frisch. Ab Initio Calculation of Vibrational Absorption and Circular Dichroism Spectra Using Density Functional Force Fields. *The Journal of Physical Chemistry*, 98(45):11623–11627, Nov. 1994. ISSN 0022-3654. doi: 10.1021/j100096a001. URL <https://doi.org/10.1021/j100096a001>. Publisher: American Chemical Society.
- [58] F. Neese. Software update: The ORCA program system—Version 5.0. *WIREs Computational Molecular Science*, 12(5):e1606, 2022. ISSN 1759-0884. doi: 10.1002/wcms.1606. URL <https://onlinelibrary.wiley.com/doi/abs/10.1002/wcms.1606>. _eprint: <https://onlinelibrary.wiley.com/doi/pdf/10.1002/wcms.1606>.
- [59] S. Spicher and S. Grimme. Robust Atomistic Modeling of Materials, Organometallic, and Biochemical Systems. *Angewandte Chemie International Edition*, 59(36):15665–15673, 2020. ISSN 1521-3773. doi: 10.1002/anie.202004239. URL <https://onlinelibrary.wiley.com/doi/abs/10.1002/anie.202004239>. _eprint: <https://onlinelibrary.wiley.com/doi/pdf/10.1002/anie.202004239>.
- [60] B. Huang and O. A. von Lilienfeld. Quantum machine learning using atom-in-molecule-based fragments selected on the fly. *Nature Chemistry*, 12:945–951, Sept. 2020. ISSN 1755-4349. doi: 10.1038/s41557-020-0527-z. URL <https://www.nature.com/articles/s41557-020-0527-z>. 24 citations (Crossref) [2021-10-21] Publisher: Nature Publishing Group QID: Q99418783.
- [61] S. Grimme, C. Bannwarth, and P. Shushkov. A Robust and Accurate Tight-Binding Quantum Chemical Method for Structures, Vibrational Frequencies, and Noncovalent Interactions of Large Molecular Systems Parametrized for All spd-Block Elements ($Z = 1-86$). *Journal of Chemical Theory and Computation*, 13(5): 1989–2009, May 2017. ISSN 1549-9618. doi: 10.1021/acs.jctc.7b00118. URL <https://doi.org/10.1021/acs.jctc.7b00118>. Publisher: American Chemical Society.
- [62] S. Grimme, J. G. Brandenburg, C. Bannwarth, and A. Hansen. Consistent structures and interactions by density functional theory with small atomic orbital basis sets. *The Journal of Chemical Physics*, 143(5): 054107, Aug. 2015. ISSN 0021-9606. doi: 10.1063/1.4927476. URL <https://doi.org/10.1063/1.4927476>.
- [63] J. G. Brandenburg, C. Bannwarth, A. Hansen, and S. Grimme. B97-3c: A revised low-cost variant of the B97-D density functional method. *The Journal of Chemical Physics*, 148(6):064104, Feb. 2018. ISSN 0021-9606. doi: 10.1063/1.5012601. URL <https://doi.org/10.1063/1.5012601>.
- [64] N. Mardirossian and M. Head-Gordon. Mapping the genome of meta-generalized gradient approximation density functionals: The search for B97M-V. *The Journal of Chemical Physics*, 142(7):074111, Feb. 2015. ISSN 0021-9606. doi: 10.1063/1.4907719. URL <https://doi.org/10.1063/1.4907719>.

- [65] S. Ehlert, U. Huniar, J. Ning, J. W. Furness, J. Sun, A. D. Kaplan, J. P. Perdew, and J. G. Brandenburg. r2SCAN-D4: Dispersion corrected meta-generalized gradient approximation for general chemical applications. *The Journal of Chemical Physics*, 154(6):061101, Feb. 2021. ISSN 0021-9606. doi: 10.1063/5.0041008. URL <https://doi.org/10.1063/5.0041008>.
- [66] Y. Zhao and D. G. Truhlar. The M06 suite of density functionals for main group thermochemistry, thermochemical kinetics, noncovalent interactions, excited states, and transition elements: two new functionals and systematic testing of four M06-class functionals and 12 other functionals. *Theoretical Chemistry Accounts*, 120(1):215–241, May 2008. ISSN 1432-2234. doi: 10.1007/s00214-007-0310-x. URL <https://doi.org/10.1007/s00214-007-0310-x>.
- [67] N. Mardirossian and M. Head-Gordon. ω B97X-V: A 10-parameter, range-separated hybrid, generalized gradient approximation density functional with nonlocal correlation, designed by a survival-of-the-fittest strategy. *Physical Chemistry Chemical Physics*, 16(21):9904–9924, May 2014. ISSN 1463-9084. doi: 10.1039/C3CP54374A. URL <https://pubs.rsc.org/en/content/articlelanding/2014/cp/c3cp54374a>. Publisher: The Royal Society of Chemistry.
- [68] N. Mardirossian and M. Head-Gordon. ω B97M-V: A combinatorially optimized, range-separated hybrid, meta-GGA density functional with VV10 nonlocal correlation. *The Journal of Chemical Physics*, 144(21):214110, June 2016. ISSN 0021-9606. doi: 10.1063/1.4952647. URL <https://doi.org/10.1063/1.4952647>.
- [69] G. Santra, N. Sylvetsky, and J. M. L. Martin. Minimally Empirical Double-Hybrid Functionals Trained against the GMTKN55 Database: revDSD-PBEP86-D4, revDOD-PBE-D4, and DOD-SCAN-D4. *The Journal of Physical Chemistry A*, 123(24):5129–5143, June 2019. ISSN 1089-5639. doi: 10.1021/acs.jpca.9b03157. URL <https://doi.org/10.1021/acs.jpca.9b03157>. Publisher: American Chemical Society.
- [70] J.-D. Chai and M. Head-Gordon. Long-range corrected double-hybrid density functionals. *The Journal of Chemical Physics*, 131(17):174105, Nov. 2009. ISSN 0021-9606. doi: 10.1063/1.3244209. URL <https://doi.org/10.1063/1.3244209>.
- [71] W. Klopper, F. R. Manby, S. Ten-no, and E. F. Valeev. R12 methods in explicitly correlated molecular electronic structure theory. *Int. Rev. Phys. Chem.*, 25:427, 2006. doi: 10.1080/01442350600799921.
- [72] S. Ten-no and J. Noga. Explicitly correlated electronic structure theory from R12/F12 ansätze. *WIREs Comput. Mol. Sci.*, 2:114–125, 2012. doi: 10.1002/wcms.68.
- [73] C. Hättig, W. Klopper, A. Köhn, and D. P. Tew. Explicitly correlated electrons in molecules. *Chem. Rev.*, 112:4–74, 2012. doi: 10.1021/cr200168z.
- [74] K. A. Peterson, T. B. Adler, and H.-J. Werner. Systematically convergent basis sets for explicitly correlated wavefunctions: The atoms H, He, B–Ne, and Al–Ar. *The Journal of Chemical Physics*, 128(8):084102, Feb. 2008. ISSN 0021-9606. doi: 10.1063/1.2831537. URL <https://doi.org/10.1063/1.2831537>.
- [75] J. Noga, S. Kedzuch, and J. Simunek. Second order explicitly correlated R12 theory revisited: A second quantization framework for treatment of the operators’ partitionings. *J. Chem. Phys.*, 127:034106, 2007.
- [76] G. Knizia and H.-J. Werner. Explicitly correlated RMP2 for high-spin open-shell reference states. *J. Chem. Phys.*, 128:154103, 2008.
- [77] T. B. Adler, G. Knizia, and H.-J. Werner. A simple and efficient CCSD(T)-F12 approximation. *J. Chem. Phys.*, 127:221106, 2007.
- [78] T. H. Dunning, Jr. Gaussian basis sets for use in correlated molecular calculations. I. The atoms boron through neon and hydrogen. *J. Chem. Phys.*, 90:1007–1023, 1989.
- [79] R. A. Kendall, T. H. Dunning, Jr., and R. J. Harrison. Electron affinities of the first-row atoms revisited. Systematic basis sets and wave functions. *J. Chem. Phys.*, 96:6796–6806, 1992.
- [80] T. H. Dunning, Jr., K. A. Peterson, and A. K. Wilson. Gaussian basis sets for use in correlated molecular calculations. X. The atoms aluminum through argon revisited. *J. Chem. Phys.*, 114:9244–9253, 2001.
- [81] E. Papajak, J. Zheng, X. Xu, H. R. Leverentz, and D. G. Truhlar. Perspectives on Basis Sets Beautiful: Seasonal Plantings of Diffuse Basis Functions. *Journal of Chemical Theory and Computation*, 7(10):3027–3034, Oct. 2011. ISSN 1549-9618. doi: 10.1021/ct200106a. URL <https://doi.org/10.1021/ct200106a>. Publisher: American Chemical Society.

- [82] K. A. Peterson and T. H. Dunning, Jr. Accurate correlation consistent basis sets for molecular core-valence correlation effects: The second row atoms Al–Ar, and the first row atoms B–Ne revisited. *J. Chem. Phys.*, 117:10548–10560, 2002.
- [83] A. Karton. Post-ccsd(t) contributions to total atomization energies in multireference systems. *J. Chem. Phys.*, 149:034102, 2018.
- [84] D. Feller, K. A. Peterson, and B. Ruscic. Improved accuracy benchmarks of small molecules using correlation consistent basis sets. *Theor. Chem. Acc.*, 133:1407, 2014.
- [85] K. A. Peterson, D. Feller, and D. A. Dixon. Chemical accuracy in ab initio thermochemistry and spectroscopy: Current strategies and future challenges. *Theor. Chem. Acc.*, 131:1079, 2012.
- [86] D. Feller, K. A. Peterson, and D. A. Dixon. A survey of factors contributing to accurate theoretical predictions of atomization energies and molecular structures. *J. Chem. Phys.*, 129:204105, 2008.
- [87] D. Feller and K. A. Peterson. Probing the limits of accuracy in electronic structure calculations: Is theory capable of results uniformly better than “chemical accuracy”? *J. Chem. Phys.*, 126:114105, 2007.